RSC Advances

COMMUNICATION

View Article Online
View Journal | View Issue

Cite this: *RSC Adv.*, 2015, **5**, 41120

Received 19th March 2015
Accepted 21st April 2015

DOI: 10.1039/c5ra04893a

www.rsc.org/advances

Fabrication of different crystallographically oriented TiO_2 nanotube arrays used in dye-sensitized solar cells

Liujie Wang,[abc] Yi Wang,[b] Yong Yang,*[ab] Xiaodong Wen,[ab] Hongwei Xiang*[ab] and Yongwang Li[ab]

Different crystallographically oriented TiO_2 nanotube arrays (NTAs) were successfully fabricated *via* the anodization of Ti film sputtered on indium tin oxide (ITO) glass. The results indicate that the preferred orientation of TiO_2 NTAs with a texture degree $f > 0.9$ for anatase (004) can be assembled over a wide range of water content in the electrolyte from 1.5 to 6.0 vol%. When the water content is more than 8 vol%, the anatase TiO_2 NTA further transforms to a polycrystal type. When compared to the characteristics of DSSCs based on the different oriented TiO_2 NTAs, the (004) preferred orientation of TiO_2 NTAs possesses the highest power conversion efficiency (PCE) and electron transport rate owing to its excellent orientation.

1. Introduction

Highly ordered TiO_2 nanotube arrays (NTAs), which can be fabricated by the anodization of a Ti foil, have been widely applied in many fields, including photocatalysis,[1] solar energy conversion[2–4] and biomedicine.[5,6] TiO_2 NTAs have uniform nanotubular structures perpendicular to the matrix. In order to optimize the function of TiO_2 NTAs in various applications, control over the morphology of the TiO_2 NTAs is regarded as one of the most important factors. Many novel TiO_2 nanotube structures, such as bamboo-type TiO_2 NTAs,[7,8] double-wall TiO_2 NTAs[9,10] and hierarchically branched TiO_2 NTAs,[11,12] have brought great interest to researchers. Bamboo-type TiO_2 NTAs used as a photoanode can substantially increase the light-to-electric energy conversion efficiency of NT-based dye-sensitized solar cells (DSSCs).[7] These types of TiO_2 NTAs grew perpendicularly to the opaque Ti metal substrate. When the TiO_2 NTA on opaque Ti foil was directly used as a DSSC, the incidental light must pass through the counter-electrode and light-absorbing electrolyte.[13] It was found that back-side illumination caused considerable light loss and was not suitable for achieving high power conversion efficiency (PCE). To overcome this drawback,[14,15] TiO_2 NTA film prepared on Ti metal can be transferred to a transparent conducting oxide (TCO) substrate[16,17] or the TiO_2 NTA prepared *via* the anodization of Ti film sputtered on a TCO substrate.[18,19] It can be no the TiO_2 NTAs prepared by anodizing from Ti foil or Ti film were amorphous and can be transformed into a polycrystal but not crystallographically oriented phase after an annealing process.[3,4,8,19] Despite numerous studies on the amorphous-to-crystalline transformation of TiO_2 nanotubes, the mechanism of the phase transformation is not well understood to date[20] and there is still little recognization for the formation of oriented TiO_2 NTAs and their application in DSSCs.

In the present study, the anatase (004) preferred oriented TiO_2 NTAs were fabricated by the anodization of Ti film (with (002) orientation) sputtered on ITO glass. The crystallographical orientation of the TiO_2 NTA could be transformed controllably *via* adjusting the water content in the electrolyte under the same annealing conditions. In addition, the texture degree f of the (004) orientation was introduced to quantitatively estimate the crystal orientation of the TiO_2 NTAs. The different oriented TiO_2 NTAs with the same thickness were assembled into DSSCs, which showed different PCE values.

2. Experimental section

Ti films were deposited on a commercial ITO glass substrate (10 Ω square^{-1}, Zh-Kv Co., Ltd.) using a radio frequency (RF) sputtering system fitted with a Ti target of 99.99% purity. The sputtering chamber was pumped down to a pressure of 10^{-3} mTorr before argon gas was introduced. Sputtering was conducted in an argon atmosphere at 10 mTorr with an applied RF power of 150 W and substrate temperature of 400 °C. During the deposition process, the target-substrate distance was kept at 50 mm and the negative dc self-bias voltage was 10 V.

[a]*State Key Laboratory of Coal Conversion, Institute of Coal Chemistry, Chinese Academy of Sciences, Taiyuan 030001, Shanxi, P.R. China. E-mail: yyong@sxicc.ac.cn; hwxiang@sxicc.ac.cn; Fax: +86 10 69667653; Tel: +86 10 69667699*

[b]*National Energy Center for Coal to Clean Fuels, Synfuels China Co., Ltd., Huairou District, Beijing 101400, P.R. China*

[c]*University of Chinese Academy of Sciences, Beijing 100049, P.R. China*

In a two-electrode cell, the TiO_2 NTAs were fabricated by anodizing Ti film in an ethylene glycol electrolyte[21] containing 0.75 wt% NH_4F and 1.5–12 vol% H_2O at room temperature. The Ti film deposited on the ITO glass was used as the anode and Pt foil (4 cm × 5 cm) was used as the counter electrode (cathode). In a 500 mL PTFE beaker, the anode and cathode were kept at a distance of 4 cm. The exposed surface area of the anode and cathode to the electrolyte was 2 cm^2 and 8 cm^2, respectively. Anodized voltages in the range of 40–60 V were employed in the process and the initial current was 0.1 A. After being anodized, the as-prepared samples were rinsed with water and dried under an air atmosphere. Anatase phase TiO_2 NTAs were obtained by annealing the anodized samples in a tube furnace with ambient air, which was heated at a ramping rate of 5 °C min^{-1} up to 450 °C, maintained at this temperature for 3 h and then cooled down to room temperature. These annealed TiO_2 NTAs firstly were soaked in a 0.5 × 10^{-3} mol L^{-1} N719 dye solution in ethanol for 24 h and ethanol was used to rinse the unabsorbed dye. The electrolyte and Pt electrode used for the DSSC were purchased from Dalian Heptachroma Solar Tech Co., Ltd., China. The DSSCs were assembled with the dye-sensitized TiO_2 NTAs and Pt electrode using a hot-melt film.

The surface morphology and crystalline phase of the TiO_2 NTAs were studied using field emission scanning electron microscopy (FESEM, FEI Quanta 400F), X-ray diffraction (XRD) spectroscopy (Bruker D2) and high-resolution transmission electron microscopy (HR-TEM, JEM-2010). The X-ray diffraction (XRD) patterns were obtained with a Bruker D2 diffractometer using Cu Kα radiation (λ = 1.5418 Å, 30 kV, 10 mA) in the scan range from 10° to 90° with a step size of 0.02° and residence time of 0.5 s. Current–voltage characteristics of the solar cells were measured under one sun condition using a solar light simulator (Newport 91160) operating at AM 1.5. Intensity modulated photocurrent/photovoltage spectroscopy (IMPS/IMVS) measurements were carried out on an electrochemical workstation (Autolab, PGSTAT302N) with a frequency response analyzer under a modulated red light emitting diode (625 nm) driven by a source supply (Autolab dynamic load interface, DYN 7412), which could provide both the dc and ac components of the illumination. The modulated light intensity was 10% or less than the base light intensity. The frequency range was set from 1 kHz to 0.01 Hz.

3. Results and discussion

Fig. 1a shows the XRD patterns of ITO glass, sputtered Ti film, non-annealed and annealed TiO_2 NTAs. The XRD pattern of Ti film sputtered on an ITO glass substrate indicates a (002) preferred orientation and the peak of the Ti film could be indexed to hexagonal titanium (JCPDS no. 44-1294). The non-annealed TiO_2 NTA does not have diffraction peaks showing an amorphous characteristic and was prepared in an electrolyte containing 2 vol% H_2O. After TiO_2 NTA was annealed under ambient air at 450 °C for 3 h, it was converted into its crystalline form. The (101) and (004) peaks of the annealed TiO_2 NTAs could be indexed to the TiO_2 anatase phase (JCPDS no. 21-1272). In addition, it is important to note that the anatase TiO_2 NTA (see Fig. 1) was in the (004) preferred orientation. Fig. 1b shows a schematic of the electrochemical cell used in the anodization of the Ti film.

To review other studies on synthesizing TiO_2 NTAs, amorphous TiO_2 NTAs have been reported to be transformed into a polycrystal form *via* a post-annealing process.[4,8,19] Hong[22] and Lee[23] fabricated the anatase (004) preferred orientation of TiO_2 NTAs by the anodization of opaque Ti foil and the as-prepared TiO_2 NTAs were not suitable for achieving high-efficiency DSSCs.[13] Herein, we have successfully synthesized the transparent (004) preferred orientation of TiO_2 NTAs *via* anodizing a (002) oriented Ti film.

Fig. 2a displays the top-view of the TiO_2 NTAs obtained on ITO glass, which are prepared in an ethylene glycol electrolyte containing 0.75 wt% NH_4F and 2 vol% H_2O. The top morphology of the TiO_2 NTA is presented in Fig.2a and the average nanotube pore diameters and wall thicknesses are roughly ~70 nm and ~10 nm, respectively. From the cross-sectional view of the TiO_2 TNAs shown in Fig. 2b and c, we can see that the TiO_2 NTAs are perpendicular to the ITO glass with smooth walls. Fig. 2d and e present a cross-sectional TEM

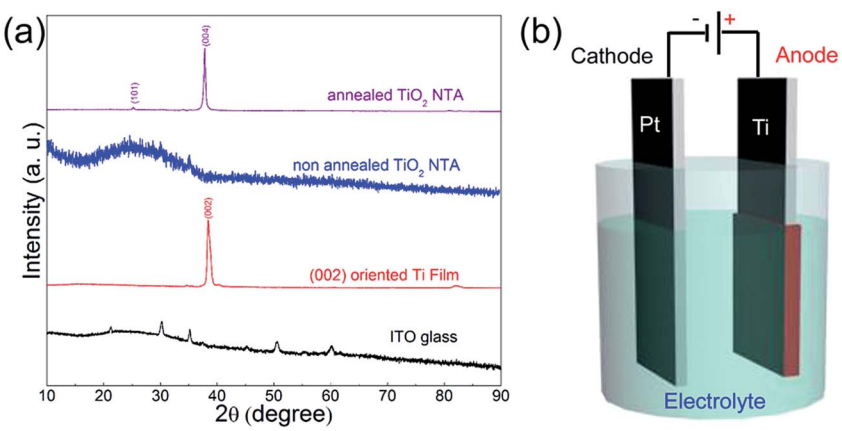

Fig. 1 (a) XRD patterns of ITO glass, RF sputtered Ti film, non-annealed and annealed TiO_2 NTAs. (b) Schematic of the electrochemical cell used in the anodization of the Ti film.

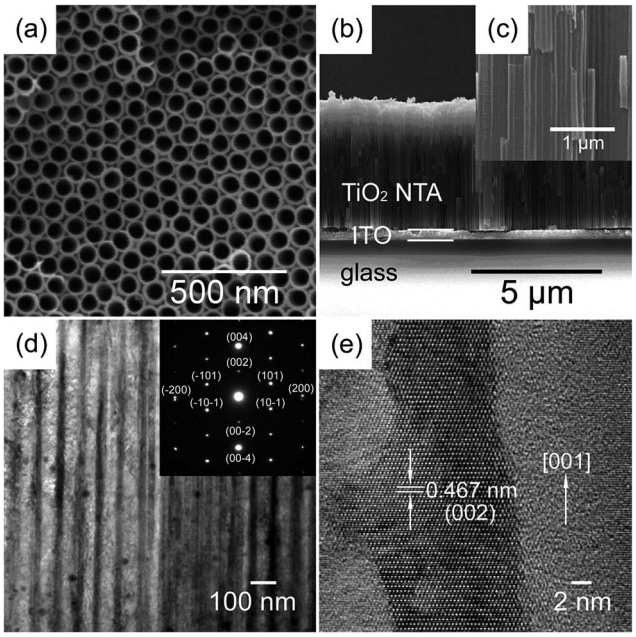

Fig. 2 SEM images of the TiO_2 NTAs. (a) Top view of the TiO_2 NTAs, (b) and (c) cross-sectional views of the TiO_2 NTAs. TEM and SAED images of the TiO_2 NTAs. (d) Cross-sectional TEM image. The inset shows the SAED pattern of the TiO_2 NTAs. (e) HR-TEM lattice image of the TiO_2 nanotube wall.

image and corresponding selected-area electron diffraction (SAED) pattern of the TiO_2 NTA and a HR-TEM image of the TiO_2 nanotube wall. In Fig. 2d, the TiO_2 NTAs show characteristic tubular structures with uniform diameter. The HR-TEM image of the nanotube wall displayed in Fig. 2e indicates that its lattice fringe was parallel to the mouth of the tube with an interplanar spacing of 0.467 nm referring to the (002) plane of the anatase phase.[24] In Fig. 2d, the SAED pattern from the cross-section of the TiO_2 NTAs indicates that the [001] orientation was parallel to the longitudinal direction of the tubes. The diffraction pattern with bright intense spots illustrates that the TiO_2 nanotube wall possessed an excellent preferred orientation, which is in good agreement with the aforementioned XRD results.

Fig. 3a shows that the XRD patterns of the TiO_2 NTAs prepared from a Ti film with (002) preferred orientation *via* anodizing in an electrolyte with a water content from 1.5 vol% to 12.0 vol%. When water content ranges from 1.5 vol% to 7.0 vol%, anatase TiO_2 NTAs with a (004) preferred orientation are formed. When the water content is ~8 vol%, anatase TiO_2 NTAs with both a (101) and (004) texture orientation can be obtained. After 9.0 vol%, the anatase TiO_2 NTAs exhibits a polycrystal type. In the abovementioned experiments, the anodized voltage was adjusted from 40 V to 60 V when the water content exceeded 5.0 vol%, which was carried out in order to obtain transparent TiO_2 NTAs. This was different to the study by Hong[22] who reported that the anatase (004) preferred orientation of TiO_2 NTAs could only be produced within a limited range of water content of around 2 wt% in the electrolyte. Our experimental results shows that the anatase (004) preferred orientation of TiO_2 NTAs can be facilely prepared in an electrolyte containing a wider range of water content (approximately 1.5–7.0 vol%). We propose that the precursor used to prepare the TiO_2 NTAs caused this difference.

To date, the mechanism of the generation of different orientations found with differing the water content in the electrolyte is not fully understood. However, in previous studies[25–28] on anodization, it is accepted that water is usually a source of oxygen in the anodizing solutions. While the exact mechanism by which water contributes oxygen to an anodic oxide film is not well-understood, strong evidence has been found for hydroxyl ion injection from the electrolyte into the anodic oxide film during anodization. When more water is present, hydroxyl ions are injected into the body of the oxide layer. So along with water content increasing in the electrolyte, more hydroxyl ions are injected into the body of the oxide. Therefore, during an annealing process, the increased number of incorporated hydroxyl ions may hinder the direction of the crystallization process into well-oriented nanograins. Further study on the role of hydroxyl groups on the crystallization behavior is on going in our research group.

In previous studies,[22,23] the quantitative evaluation of the texture degree for the (004) orientation was not considered. According to our experiments in this study, the texture degree *f* of the (004) orientation was defined to further evaluate the

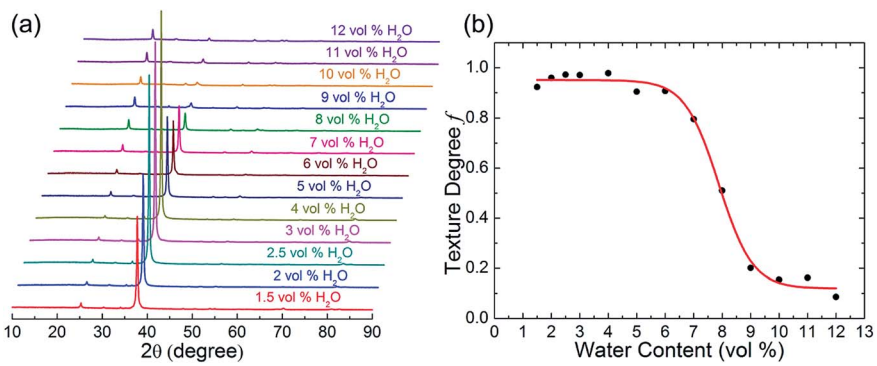

Fig. 3 (a) XRD patterns of the annealed TiO_2 NTAs fabricated in an ethylene glycol electrolyte containing 0.75 wt% NH_4F and 1.5–12.0 vol% H_2O with anodization voltages in the range of 40–60 V. (b) Evolution of texture degree *f* of the (004) orientation *versus* water content.

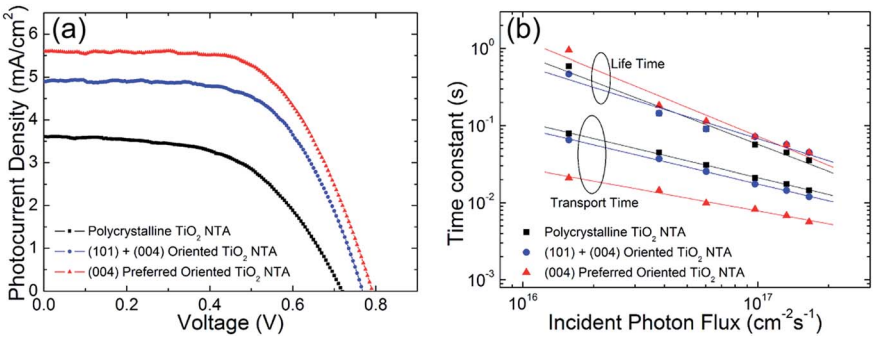

Fig. 4 (a) Photocurrent–voltage (J–V) curves for the DSSCs based on the different orientations of the TiO_2 NTAs and (b) electron transport time and lifetime for the DSSCs on the different orientations of the TiO_2 NTAs.

anatase phase TiO_2 NTAs with different preferred orientations found with differing the water content in the electrolyte. The texture degree f was estimated using the Lotgering method:[29]

$$f = (P_{(001)} - P_0)/(1 - P_0),$$

where $P_{(001)} = \sum I_{(001)}/\sum I_{(hkl)}$ and $P_0 = \sum I_{0(001)}/\sum I_{0(hkl)}$. $\sum I_{(001)}$ is the summation of the XRD peak intensities of all the (001) peaks (*i.e.*, 001, 002…) in the textured sample pattern. $\sum I_{(hkl)}$ is the summation of the peak intensities of all (hkl) peaks, which appears in the XRD pattern. $\sum I_{0(001)}$ and $\sum I_{0(hkl)}$ are the standard random powder using the published diffraction file JCPDS no. 21-1272. Diffraction peaks in the 2θ range of 10°–90° are considered in the calculation.

$f = 0$ and $f = 1$ correspond to the typical polycrystal and complete (001) texture cases, respectively, and $0 < f < 1$ for partial texture. Fig. 3b shows the evolution of f *versus* water content. When the water content ranges from 1.5 vol% to 6.0 vol%, all values of f are greater than 0.9. This illustrates that the anatase TiO_2 NTAs possess an excellent (004) preferred orientation. The value of f drops to 0.79 when the water content increases to 7.0 vol%. When the water content increases to 9.0 vol%, the value of f sharply decreases to 0.2, indicating that the anatase (004) preferred orientation of the TiO_2 NTAs transformed to a polycrystal type.

The three different orientations of the TiO_2 NTAs (lengths up to 5 μm) are assembled into solar cells as described in the Experimental section. Fig. 4a presents the current–voltage curves for the DSSCs based on the three photoanodes. The DSSC based on the (004) preferred orientation of TiO_2 NTAs shows an open-circuit voltage (V_{oc}) of 0.79 V, short-circuit current density (J_{sc}) of 5.59 mA cm^{-2} and a PCE (η) of 2.69%. In contrast, the V_{oc}, J_{sc} and η of DSSC based on double-texture TiO_2 NTA is 0.765 V, 4.89 mA cm^{-2} and 2.32%, respectively. The V_{oc}, J_{sc} and η of the DSSC based on polycrystalline TiO_2 NTA were 0.72 V, 3.60 mA cm^{-2} and 1.43%, respectively. It can be noted that the (004) preferred orientation of the TiO_2 NTAs yields the highest conversion efficiency and highest J_{sc} than the other orientations of the TiO_2 NTAs studied. In order to evaluate the main factors for the different performance of the different orientations of the TiO_2 NTAs, the electron transport characteristics were measured and compared. Fig. 4b shows the IMPS and IMVS results for the three structures. There are a very interesting finding from the IMPS measurements shown in Fig. 4b in which the electron transport time in the (004) preferred orientation of the TiO_2 NTAs was shorter (≈3 times) than in the other orientations of the TiO_2 NTAs studied. This result may be ascribed to the regular arrangement of the grains along the [001] orientation in the nanotube wall, which was the main reason to remarkably decrease the defect component of the tube wall.[30] Due to the highest electron transport rate for the (004) preferred orientation of the TiO_2 NTAs, the J_{sc} of the (004) orientated TiO_2 NTAs was the highest of the three different orientations of the TiO_2 NTAs studied. A similar lifetime was observed for three different orientations of the TiO_2 NTAs, as shown in Fig. 4b and the results indicate that the same potential surface recombination sites exist in the three different samples. Therefore, the DSSCs based on the (004) orientated TiO_2 NTAs possesses the highest PCE value.

4. Conclusions

In summary, the anatase (004) preferred orientation of TiO_2 NTAs can be fabricated in a controlled manner from a (002) preferred orientated Ti film *via* anodization over a wide range of water content in the electrolyte of 1.5–7.0 vol%. The HR-TEM and SAED patterns of the TiO_2 NTAs indicate that the [001] orientation was parallel to the longitudinal direction of the tubes with their preferred orientation. When the water content was ~8 vol%, anatase TiO_2 NTAs with both (101) and (004) texture orientations can be obtained. After 9.0 vol%, the anatase TiO_2 NTAs exhibit a polycrystal type. The three different oriented TiO_2 NTAs were assembled to DSSCs and used as photoanodes, in which the (004) preferred orientation of the TiO_2 NTAs exhibited the highest PCE, which was attributed to its highest electron transport rate resulting from the regular arrangement of grains along the [001] orientation in the nanotube walls. It is expected that this strategy used for the fabrication of preferred orientations of TiO_2 NTAs has great potential for application in highly efficient DSSCs through further interface modification engineering.

Acknowledgements

This study was supported by the National Basic Research Program of China (973 Program, 2011CB201401), the National

High Technology Research and Development Program of China (863 Program, 2011AA05A205) and Synfuels China Co., Ltd.

Notes and references

1 C. Xu, Y. Song, L. F. Lu, C. W. Cheng, D. F. Liu, X. H. Fang, X. Y. Chen, X. F. Zhu and D. D. Li, *Nanoscale Res. Lett.*, 2013, **8**, 391.
2 N. Liu, K. Lee and P. Schmuki, *Electrochem. Commun.*, 2012, **15**, 1.
3 M. D. Ye, X. K. Xin, C. J. Lin and Z. Q. Lin, *Nano Lett.*, 2011, **11**, 3214.
4 M. D. Ye, D. J. Zheng, M. Q. Lv, C. Chen, C. J. Lin and Z. Q. Lin, *Adv. Mater.*, 2013, **25**, 3039.
5 B. S. Smith, S. Yoriya, L. Grissom, C. A. Grimes and K. C. Popat, *J. Biomed. Mater. Res., Part A*, 2010, **95**, 350.
6 W. T. Peng, Z. M. Qiao, Q. Zhang, X. D. Cao, X. F. Chen, H. Dong, J. W. Liao and C. Y. Ning, *J. Mater. Chem. B.*, 2013, **1**, 3506.
7 D. Kim, A. Ghicov, S. P. Albu and P. Schmuki, *J. Am. Chem. Soc.*, 2008, **130**, 16454.
8 S. R. Albu, D. Kim and P. Schmuki, *Angew. Chem., Int. Ed.*, 2008, **47**, 1916.
9 S. P. Albu, A. Ghicov, S. Aldabergenova, P. Drechsel, D. LeClere, G. E. Thompson, J. M. Macak and P. Schmuki, *Adv. Mater.*, 2008, **20**, 4135.
10 Y. J. Ji, K. Ch. Lin, H. G. Zheng, J. J. Zhu and A. C. S. Samia, *Electrochem. Commun.*, 2011, **13**, 1013.
11 Z. Jin, G. T. Fei, X. Y. Hu, S. H. Xu and L. D. Zhang, *Chem. Lett.*, 2009, **38**, 288.
12 B. Chen and K. Lu, *Langmuir*, 2012, **28**, 2937.
13 J. Y. Kim, J. H. Noh, K. Zhu, A. F. Halverson, N. R. Neale, S. Park, K. S. Hong and A. J. Frank, *ACS Nano*, 2011, **5**, 2647.
14 J. H. Park, T. W. Lee and M. G. Kang, *Chem. Commun.*, 2008, **25**, 2867.
15 T. Song, F. Zhang, X. J. Shen, X. H. Zhang, X. L. Zhu and B. Q. Sun, *Appl. Phys. Lett.*, 2009, **95**, 233502.
16 J. Zhang, S. Q. Li, H. Ding, Q. T. Li, B. Y. Wang, X. N. Wang and H. Wang, *J. Power Sources*, 2014, **247**, 807.
17 Z. L. He, W. X. Que, P. Sun and J. B. Ren, *ACS Appl. Mater. Interfaces*, 2013, **5**, 12779.
18 O. K. Varghese, M. Paulose and C. A. Grimes, *Nat. Nanotechnol.*, 2009, **4**, 592.
19 K. Y. Lee, R. Kirchgeorg and P. Schmuki, *J. Phys. Chem. C*, 2014, **118**, 16562.
20 D. Kowalskia, D. Kimb and P. Schmuki, *Nano Today*, 2013, **8**, 235.
21 S. L. Lim, Y. L. Liu, J. Li, E. T. Kang and Ch. K. Ong, *Appl. Surf. Sci.*, 2011, **257**, 6612.
22 S. Lee, I. J. Park, D. H. Kim, W. M. Seong, D. W. Kim, G. S. Han, J. Y. Kim, H. S. Jung and K. S. Hong, *Energy Environ. Sci.*, 2012, **5**, 7989.
23 M. H. Jung, K. C. Ko and J. Y. Lee, *J. Phys. Chem. C*, 2014, **118**, 17306.
24 J. M. Li and D. S. Xu, *Chem. Commun.*, 2010, **46**, 2301.
25 G. M. Krembs, *J. Electrochem. Soc.*, 1963, **8**, 938.
26 B. Melody, T. Kinard and P. Lessner, *Electrochem. Solid-State Lett.*, 1998, **1**, 126.
27 Y.-M. Li and L. Young, *J. Electrochem. Soc.*, 2001, **148**, B337.
28 H. E. Prakasam, K. Shankar, M. Paulose, O. K. Varghese and C. A. Grimes, *J. Phys. Chem. C*, 2007, **111**, 7235.
29 E. M. Sabolsky, S. T. McKinstry and G. L. Messing, *J. Appl. Phys.*, 2003, **93**, 4072.
30 J. V. Cab, S. R. Jang, A. F. Halverson, K. Zhu and A. J. Frank, *Nano Lett.*, 2014, **14**, 2305.